NJC

New Journal of Chemistry

A journal for new directions in chemistry

Accepted Manuscript

This article can be cited before page numbers have been issued, to do this please use: D. J. Perez Enriquez, M. L. Dell´Arciprete, M. L. Dittler, A. Miñan, E. Prieto and M. C. Gonzalez, *New J. Chem.*, 2020, DOI: 10.1039/C9NJ06414A.

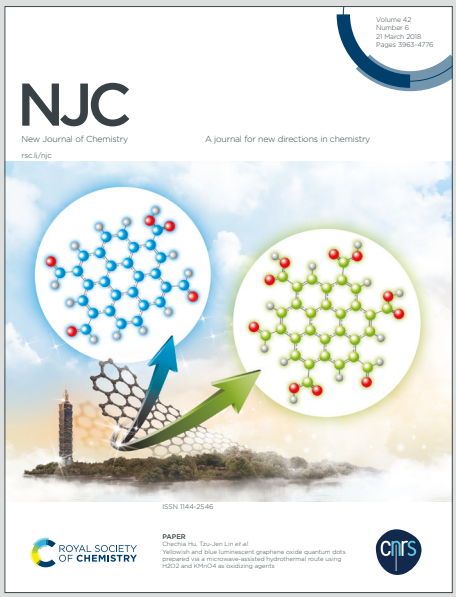

View Article Online
DOI: 10.1039/C9NJ06414A

Amorphous calcium organophosphates nanoshells as potential carriers for drug delivery to Ca^{2+}-enriched surfaces.

Darlin J. Perez Enriquez,[†] María L. Dell' Arciprete,[†,*] María L. Dittler,[†] Alejandro Miñan,[†] Eduardo Prieto,[†] and Mónica C. Gonzalez[†]

† Instituto de Investigaciones Fisicoquímicas Teóricas y Aplicadas (INIFTA), CCT-La Plata-CONICET, Universidad Nacional de La Plata, La Plata, Argentina. Diagonal 113 y 64, La Plata, Argentina.

ABSTRACT

A highly selective nanocarrier for targeted drug transport and delivery to calcium-containing surfaces, as bone mineral matrix, is described. The nanocarrier, a calcium phosphate (CaP) nanoshell, is capable of interacting with calcium ions contained in enriched surfaces (Ca^{2+} modified mica surface, hydroxyapatite nanoparticles (Ap) films on glass, and Ap modified 45S5® bioactive glass-based scaffolds) with the consequent disruption of the inorganic structure and release of (bio) molecules contained in the interior. The antibiotic Levofloxacin (LX) was used as a model drug for the encapsulation and drug release studies which allowed monitoring by fluorescence spectroscopic methods. Accumulation and disruption of CaP nanoshells triggered by calcium ions over surfaces, was followed by microscopy techniques as SEM, AFM, and fluorescence microscopy. Bacterial susceptibility and time killing assays demonstrated the bactericidal potential of the nanoshells containing LX. A mechanism for the Ca^{2+}-activated CaP nanoshell accumulation and drug release is

View Article Online
DOI: 10.1039/C9NJ06414A

proposed and discussed.

KEYWORDS: *Calcium phosphate nanoshells; Ca^{2+}activation; surface interaction; carboxyl group; drug release, bacterial susceptibility.*

1. INTRODUCTION

The development of delivery systems for drugs, proteins, DNA and genes, among others, represents an accepted and essential strategic tool for the treatment of illness. It addresses issues associated with pharmaceuticals solubility and stability in the biological environment, maintenance of the drug effective concentration, enhanced drug performance and acceptability by increasing efficacy, improving safety and patient compliance.[1,2] To meet the requirements of an effective drug delivery, vehicles are designed to control drug release at a desired target site as response of an internal or external stimuli. Internal stimuli-responsive nanocarriers release their cargo as a consequence of the specific physicochemical characteristics of the physiological targeted site as pH, redox and thermal conditions, and the presence of specific enzymes.[3] Nanoparticles of various compositions as calcium phosphate, gold, bioglass, polymer-modified porous silicon, natural polymers as chitosan and elastine, and liposomes, are among the drug nanocarriers developed to stimulate mineralization and/or promote osteoblast activity in bone tissue.[4–6] Drug delivery to bone is limited by the tissue characteristics composed by the nanoscale ensemble of minerals (~ 69%) and organic matrix, being hydroxyapatite the principal component. The local pH diminution and the increase of Ca^{2+} concentration taking place during bone resorption were considered as internal boost for drugs release.[7] In that sense, the increased solubility of CaP materials with a pH decrease motivated their use as pH-responsive carriers for drug delivery.[8]

View Article Online
DOI: 10.1039/C9NJ06414A

Liposomes comprise one of the most effective first generation nanocarriers due to their intrinsic composition and ability to encapsulate hydrophilic drugs in the aqueous core or hydrophobic molecules in the lipid bilayer. To overcome their poor mechanical stability and associated burst release, they were coated with calcium phosphates shells (CaP). [9,10] In fact, calcium phosphate materials have received much interest in the field of drug delivery due to their excellent biocompatibility and biodegradability in biological systems, as well as the ability to promote osteoblast adhesion and osteoconductivity, [7,10–13] at the time it provides the nanocarrier of a surface capable of being functionalized for active targeting.[8]

In the aim of designing a bone responding nanocarrier, we evaluated the response of carboxylic-functionalized calcium phosphate (CaP) coated 1,2-dioleoyl-sn-glycero-3-phosphate (DOPA) liposomes [10] herein denoted CaPLi, towards Ca^{2+} enriched surfaces. To that purpose, the encapsulation and delivery of the third generation fluoroquinolonic antibiotic Levofloxacin (LX) was examined. CaPLi vehicles carrying the antibiotic LX are denoted CaPLiLX. Fig. 1 shows a scheme of the developed LX-loaded nanocarrier system.

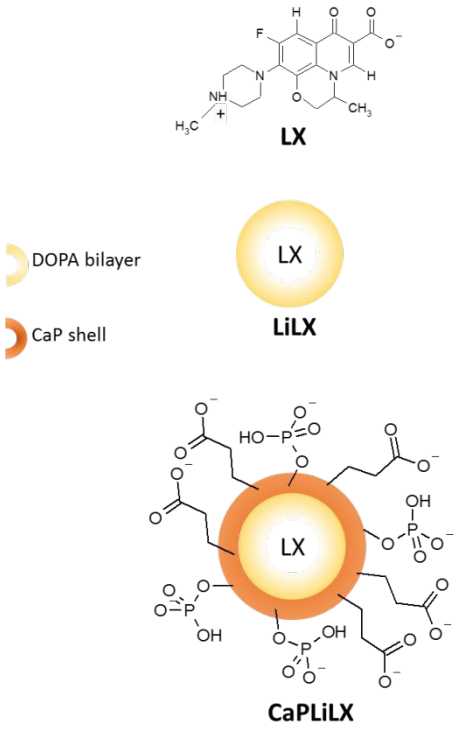

Fig. 1. Chemical structure of Levofloxacin (LX) and schematic representation of the nanocarrier.

View Article Online
DOI: 10.1039/C9NJ06414A

2. EXPERIMENTAL SECTION

2.1 Materials.

Lyophilized lipids 1,2-dioleoyl-sn-Glycero-3-Phosphate (DOPA, Avanti Polar Lipids, Alabaster, Alabama, USA), Levofloxacin (LX, Sigma-Aldrich, St Louis, MO, USA), Acridine orange (AO, Sigma, St Louis, MO, USA), Calcium chloride (analytical grade, Anedra), Calcium hydroxide (98.5%, Sigma Aldrich), Sodium hydroxide (ACS, Cicarelli), Phosphoric acid (85%, Cicarelli), 2-Carboxyethanephosphonic acid (CEPA, 94%, Aldrich), Potassium Chloride (ACS, Biopack), Potassium Bromide (ACS, J.T. Baker), Sodium chloride (ACS, Anedra), Potassium phosphate dibasic (99%, Cicarelli), Chloroform (99.9%, J.T. Baker), Iron chloride (98.3%, J.T. Baker), Ammonium thiocyanate (97.5%, Cicarelli), Polyvinyl alcohol (PVA, completely hydrolyzed, MW 30000, Merck.), 45S5® and Bioactive glass (BG) commercial powder (particle size 4 µm $Na_2Ca_2Si_3O_9$, SCHOTT Ag, Standort Landshut) were used as obtained. All solutions were prepared in ultrapure water (0.055 µS cm^{-1}) obtained from an OSMOION™ purification system. Regenerated cellulose dialysis membrane Spectra/Por 1 with a MWCO of 6000-8000 Da was obtained from Spectrum Labs. For scaffolds preparation fully reticulated polyester-based Polyurethane (PU) foam with 60 ppi (pores per inch) from Deutschland (Eurofoam GmbH) was used as sacrificial template for the replication method.[14] The foam was cut in cylindrical shape with 12 mm of diameter and 7 mm in thickness.

2.2 Synthesis of Materials.

Bioactive glass-ceramic scaffolds (BGS) and *hydroxyapatite nanoparticles* (Ap) were obtained as described elsewhere.[15] Briefly, scaffolds were prepared by the polyurethane foam method using commercial 45S5 BG® particles. Hydroxyapatite nanoparticles were obtained by a wet chemical procedure using H_3PO_4 and calcium hydroxide as reactants. Surface modification of the scaffold was performed by deep-coating as described by Dittler *et al.*[15] The modified scaffolds were named Ap-BGS.

View Article Online
DOI: 10.1039/C9NJ06414A

Calcium phosphate nanoshell synthesis was performed as described in the literature with some modifications.[10] To that purpose, aqueous solutions of DOPA (1 mg/mL) and alternatively LX (100 μM or 6 μM, the latter for fluorescence measurements only) or AO (100 μM) were prepared and homogenized by vortexing until complete dissolution. The mixture was submitted to 5 cycles of 30 seconds work of tapered probe sonication at 10 W with 30 second rest. Liposome formation after sonication was suggested by a change in the opalescence of the suspension. [16] The sample was purged with Ar for 30 minutes in an ice bath and centrifuged at 12000 rpm for 5 minutes. Samples were labelled as LiLX or LiAO for LX-containing and AO-containing liposomes, respectively.

Coating of LiLX and LiAO with CaP and surface derivatized with 2-carboxyethanephosphonic acid to yield CaP-coated liposomes labeled CaPLiLX and CaPLiAO, respectively, was performed according to the protocol previously described[10] which considered the formation of a Ca^{2+} deficient calcium phosphate material. Nanoshells were stored in a dark vessel at 4 °C. Fig. 1 shows the schematic representation of the nanocarriers synthetized.

2.3 Characterization Methods.

Nanoshell formation and surface characterization were assessed by Wide Angle X-Ray Scattering (WAXS), X-Ray Diffraction (XRD), Transmission electron Microscopy (TEM), High Resolution Scanning Transmission Electron Microscopy (HR-STEM), Energy Dispersive X-ray Spectroscopy (EDS), ATR-FTIR spectroscopy, dynamic light scattering (DLS) and electrophoretic mobility (μ_e), as described in S.I. "Characterization Methods". *Photoluminescence measurements* for CaPLiLX characterization were performed using a Jobin-Yvon Spex Fluorolog FL3-11 also described in the supporting information.

Lipid quantification of LiLX was accomplished by Stewart colorimetric assay.[17] The lipid concentration on 1:10 diluted LiLX sample measured by Stewart method yielded a concentration of the order of 0.1 mg/mL, indicating that all the DOPA initially incorporated during synthesis was forming vesicles.

View Article Online
DOI: 10.1039/C9NJ06414A

Calcium quantification in CaPLiLX suspension was determined by ICP-OES using a Shimadzu ICPE-9820 instrument. The quantitative determination was performed according to EPA 6010.

LX encapsulation efficiency (EE%) of LX in the liposomes was determined as the ratio between the emission intensity upon 330 nm excitation of LX in DOPA mixtures right after vortexing and sonication (C_{LXini}) and that after liposome dialysis against ultrapure water for 24 h (C_{LXlipo}), EE% = $100 \times C_{LXlipo}/C_{LXini}$. The strategy used for the determination of the encapsulation efficiency minimizes the effects of light scattering and fluorescence quenching due to the presence of liposomes. However, since no other correction was performed, the obtained EE% is a lower limit value.

2.4 Drug release studies.

The release profiles of LX were investigated in PBS (pH 7.4) and acetate (pH 4.35) buffers, and in Simulated body fluid (SBF, pH 7.4) with ion concentrations nearly equal to those of human blood plasma. A volume of 3 mL CaPLiLX suspension (3.4 x 10^{-6}M LX after dialysis estimated from UV-vis absorption calibration curve, *see* Section 3.2 below), or alternatively 1.7x10^{-5}M LX solution, were placed in 2.7 x 4.7 cm dialysis membrane bags and immersed in 200 mL (V_0) of PBS or acetate buffers, or SBF solution. The solutions were incubated at (37 ± 1) ºC under stirring (80 rpm) up to 75 h. [18] At different time intervals, 2mL-aliquots (V_i) of the release medium were taken and replaced with the same volume of fresh media solution. The assays were performed in duplicates. The LX concentration (C_i) in the aliquots were determined by measuring the fluorescence intensity at 450 nm (PBS buffer and SBF) or 495 nm (acetate buffer) and the actual LX released concentration obtained by comparison with a fluorescence-LX concentration calibration curve in the same media. The LX release rate (RR) was calculated by $RR = (Q_n/W)$ where W is the total drug content in the original CaPLiLX samples and Q_n the cumulative released mass at each time interval n.[18] Q_n may be calculated as $Q_n = C_n \times V_0 + \sum_{i=0}^{n-1} C_i \times V_i$.

View Article Online
DOI: 10.1039/C9NJ06414A

2.5 Interaction with surfaces.

Interaction of LiLX and CaPLiLX samples with Ca^{2+}- rich mica surfaces was addressed by *Atomic Force Microscopy*. The measurement was performed in dynamic mode (tapping) thus avoiding changes induced by lateral forces. In all instances, 10 µl of the samples were dropped on freshly cleaved mica substrates with and without the previous addition of 10 µL of $CaCl_2$ 0.1 M. Samples were dried under N_2 for 10 minutes and analyzed through the use of probes doped with silicon nitride (Model RTESP, Veeco Instruments, Santa Barbara, CA, USA; tip radii, 8–12 nm, 271–311 kHz, force constant 40 N m^{-1}). Images were obtained at 25ºC with a Multi-Mode Scanning Probe Microscope (Veeco) equipped with a Nanoscope V controller (Veeco) at the typical scanning rate (1 Hz).

Interaction of CaPLiLX deposited on BGS and Ap-BGS was observed by *Scanning Electron Microscopy* (SEM) images taken using an environmental scanning electron microscope FEI Quanta 200, after 10 and 120 minutes of contact. Sample preparation involved fixation and dehydration steps. Fixation was performed by immersion of the slides in a 2% glutaraldehyde solution at 4ºC for 2 h and washed with a PBS (pH 7.4) buffer solution. Dehydration was performed by sequential immersion in cool ethanol-water mixtures (30%, 50%, 70%, 90% and 95%) followed by two immersion processes in absolute ethanol at room temperature for 20 min. Samples were treated by critical point drying in order to replace the liquids by CO_2 and further metalized with Au.

In order to confirm the nanoshell interaction with Ca^{2+} - enriched surfaces, samples carrying the dye AO were prepared as described in the experimental section and observed by *epifluorescence microscopy*. The samples were deposited over clean glass slides and Ap modified glass slides. Immediately after deposition (0 min) and after 10 and 180 minutes of contact time, the surfaces were observed with a fluorescence microscope (Olympus BX51, Olympus Corp., Tokyo, Japan) equipped with a #WB filter (dichroic mirror DM500, excitation filter BP450-480, emission filter BA515). The microscope was connected to an Olympus DP71 (Olympus Corp., Tokyo, Japan) color video camera.

Images were taken instantly after opening the microscope shutter to the computer monitor and in identical experimental conditions. The images were analyzed by Image J software.

2.6 Bacterial studies.

Bacterial suspensions. *S. aureus* ATCC-25923 was inoculated in 150 mL of sterile nutrient broth (NB, Britania, Argentina) and grown overnight with shaking (170 rpm) at (37 ± 1) ºC. The bacterial suspension was further adjusted with fresh NB to 1×10^5 bacteria/ml and used for the biological assays.

Antibiotic susceptibility assay. The minimum inhibitory concentration (MIC) of LX against planktonic *S. aureus* was performed using the broth microdilution method according to the CLSI guidelines.[19] The MIC was defined as the lowest concentration of LX at which bacterial growth was not detected after 20 h. The minimum bactericidal concentration (MBC) of LX for planktonic bacteria was determined by plate count method. The antibiotic concentration that produced 99.9% mortality was considered as the MBC. The assays were performed in triplicates from independent bacterial cultures.

In Vitro Time-Kill Experiment. Static time-kill studies were conducted to evaluate the antimicrobial activity of LX-containing nanoshells according to a previously reported method.[20] All experiments were performed with an initial *S. aureus* inoculum of ~ 5.0 x 10^4 bacteria/mL at (37 ± 1) ºC. Time-kill assays were performed in duplicate using CaPLiLX suspension and LX solution at 2x MIC (MBC, 1.0 µg/mL). At defined time intervals (0, 3, 6, 24 h), bacterial growth was quantified by plating 10-fold dilutions on nutrient agar (Britania, Argentina). Moreover, growth control was performed and consisted of a bacterial suspension with fresh NB which was enumerated in the same time interval. Finally, viable bacteria values were plotted against time for each formulation.

3. RESULTS AND DISCUSSION

3.1 Characterization of CaPLiLX samples.

HR-STEM, TEM, and SEM electron microscopy images of CaPLiLX samples (*see* Fig. 2a and b and S.I., Fig. S1) showed polydisperse spherical-shaped nanoparticles of 90-160 nm size. While a typical core-shell structure is observed in the TEM image in Fig. S1c, EDS mapping images (Fig. 2c-d) show the homogeneous distribution of Ca and P on the nanoshells.[21] The presence of N which could only be attributed to the presence of LX is also distributed uniformly in the nanospheres (Fig. 2e), thus confirming LX inclusion in CaPLiLX nanostructure. Moreover, all electron microscopy images only show the presence of nanospheres before and after CaP coating, thus strongly supporting that no CaP separate particles are formed.

The average size of 171.8 (± 0.8) nm measured by DLS for CaPLiLX suspended in aqueous suspensions is in line with the sizes observed by TEM, HR-STEM and SEM data. Therefore, a low agglomeration of CaPLiLX in aqueous suspensions may be inferred. In fact, CaPLiLX average size measured by DLS after one-week storage of the suspensions at 4 °C is of 176 (± 2) nm, thus also suggesting a good stability of CaPLiLX suspensions.

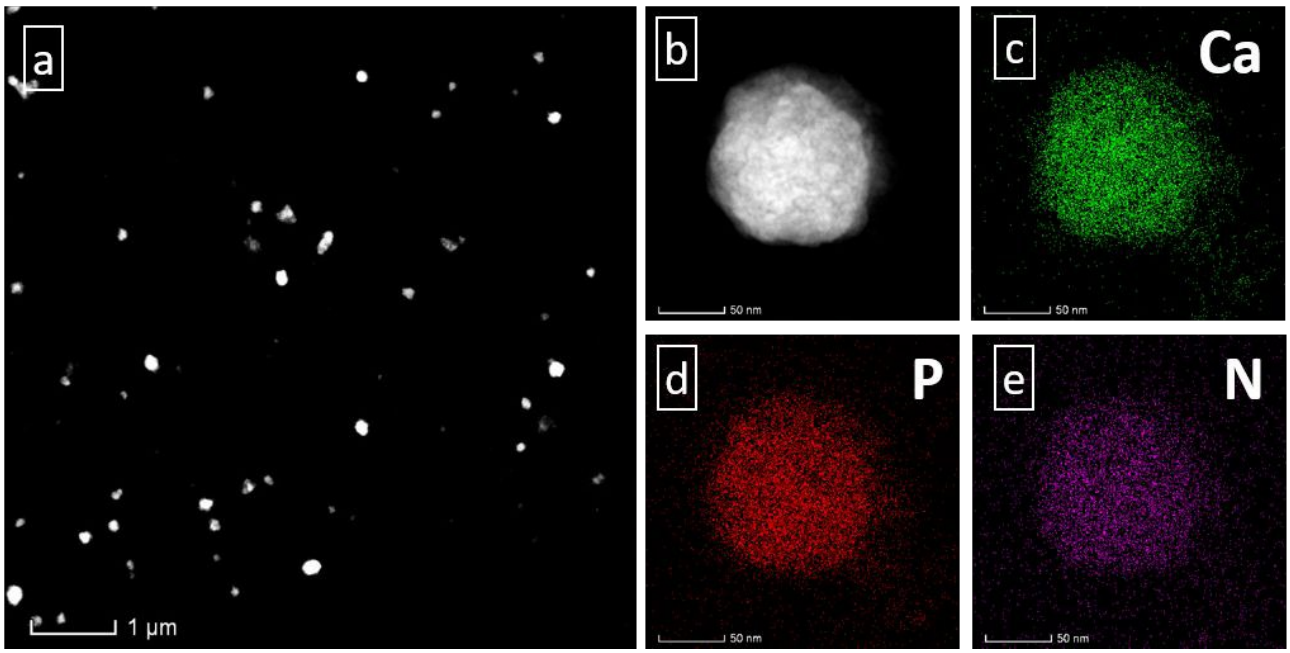

Fig. 2. HR-STEM images of CaPLiLX (a and b), EDS elemental mapping images of Ca, P and N (c, d and e, respectively).

View Article Online
DOI: 10.1039/C9NJ06414A

Fig. 3 reports the ATR-FTIR spectra of LX, DOPA, CaP nanoparticles deposited in the absence of liposomes, LiLX and CaPLiLX. LiLX samples show characteristic peaks of DOPA at 1465 cm^{-1} and 1175 cm^{-1} assigned to -CH_2 scissoring and C-O symmetric stretching of esters in the lipid structure. Other DOPA characteristic peaks at 2695 and 1740 cm^{-1} are also observed in LiLX samples, as discussed further on. LiLX depict LX characteristic bands at 1625, 1250-1300 and 1085 cm^{-1} assigned to keto oxygen in LX ring, stretching of amines and C-F group, respectively, thus confirming the simultaneous presence of LX and DOPA liposomes in the samples.

After coating LiLX with a shell of calcium phosphate, the IR-ATR spectrum of CaPLiLX exhibited bands at 896, 1060 (very intense), and 1118 cm^{-1} characteristic of the stretching vibrations of P-OH, and P-O in phosphates. Characteristic DOPA bands at 2695, 1740, and 1465 (small) cm^{-1} associated to HO- vibrations of O=P-OH[12] groups, stretching of ester carbonyls in lipids, and -CH_2 scissoring, are also observed in CaPLiLX spectra. Bands associated to the asymmetric and symmetric stretching of carboxylate groups[22] at 1577 and 1406 cm^{-1}, respectively, may be due to attached CEPA terminations on the CaPLiLX surface. The double band at 2857-2927 cm^{-1} is assigned to C-H stretching confirm the presence of carbon-chains on the nanoshell surface. Interestingly, sharp peaks at 3570 cm^{-1} due to OH stretching in highly crystalline CaP powders,[23,24] is absent in CaPLiLX spectrum. However, it should be noted that CaP nanoparticles deposited in the absence of liposomes, but otherwise identical experimental conditions, present a spectrum coincident with that of hydroxyapatite with a distinctive sharp peak at 3570 cm^{-1}. Therefore, suggesting that the CaP shell deposited on the liposome surface is amorphous. In line with this observation, XRD (*see* S.I. Fig. S2) and WAXS (see Fig. 3b) diffractograms of CaPLiLX powders and CaPLiLX aqueous suspensions, respectively, show broad and diffuse patterns characteristic of non-crystalline phases. Furthermore, no diffraction patterns were observed in HR-STEM images.[24–26]

View Article Online
DOI: 10.1039/C9NJ06414A

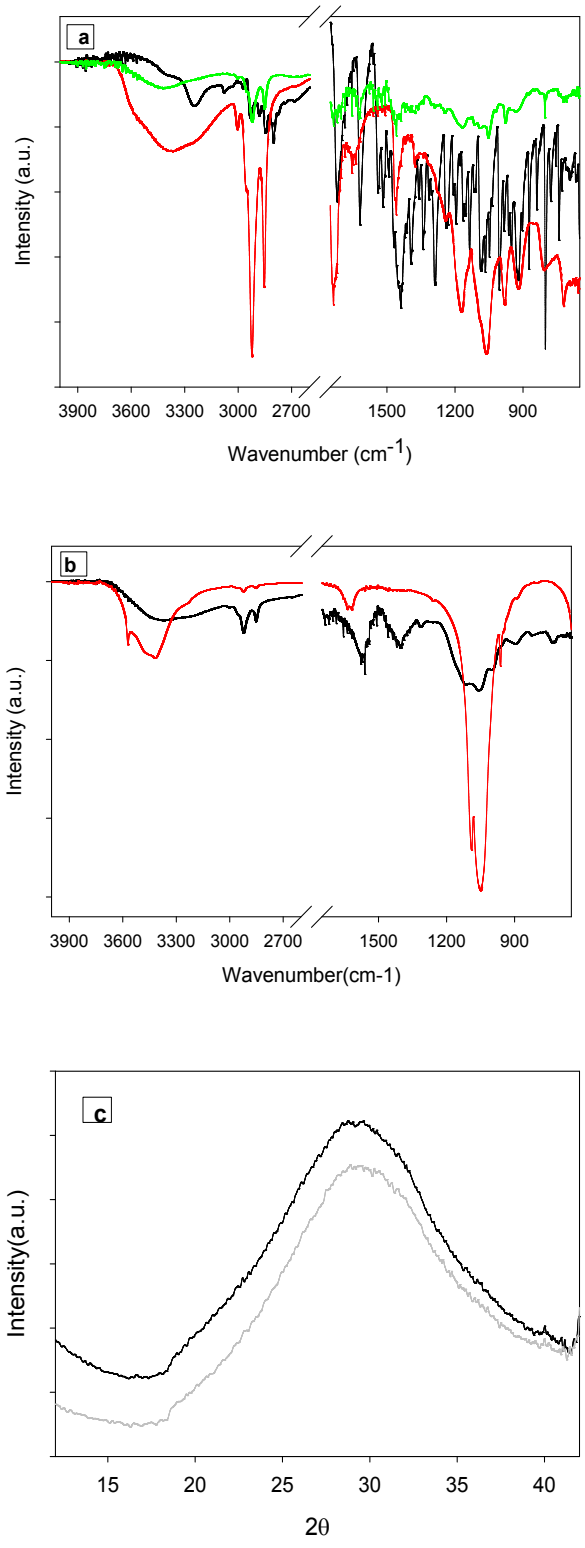

Fig. 3. (a) ATR-FTIR absorption spectra of LX (black), DOPA (red) and LiLX (green). (b) ATR-FTIR absorption spectra of CaPLiLX (black) and CaP deposited in the absence of liposomes (red). (c)

WAXS patterns obtained from CaPLiLX colloidal suspensions in the absence (black line) and in the presence (grey line) of 0.05 M of Ca^{2+} ions.

Two experimental conditions favored the precipitation of an amorphous CaP (ACP) shell. On one hand, the Ca/P molar ratio added to the liposomes in order to deposit the CaP shell is 1.0, without considering the lipids phosphate head groups. This ratio is in the lower limit range of 1 – 2.2 reported for amorphous phases.[26] On the other hand, the presence of organic compounds (such as lipids) diminish the solubility of ions due to a change in the dielectric constant of the media.[26] An increase in precipitation kinetics of Ca^{2+} and PO_4^{3-} may occur, which favors amorphization. The amorphous phase was further stabilized by surface derivatization with CEPA.

3.2 Determination of liposome and encapsulated LX concentrations.

Liposomes encapsulation of LX, as evaluated from LX absorption at 290 nm, growths with increasing solution concentration of LX up to 100 μM. Higher LX concentrations do not lead to an increased loading of the antibiotic. A minimum LX *encapsulation efficiency* of 56.5% was obtained for LX solution concentrations of 100 μM, of the order reported for LX encapsulation in nanostructured myristyl myristate lipid particles employing sonication methods [27] and for that obtained in soya lecithin/cholesterol synthesized by the so-called remote loading methods.[18]

To calculate approximately the total number of liposomes in suspension, the volume of a lipid molecule was estimated considering the approximation postulated by Koenig for unsaturated phosphatidylcholine lipids in the liquid crystalline lamellar phase. The equation $V_L(T) = V_H + n_{CH}x\ V_{CH}(T) + n_{CH2}xV_{CH2}(T) + n_{CH3}xV_{CH3}$ was used to estimate a volume of ~1300 Å^3 for a DOPA molecule, where n_{CH}, n_{CH2} and n_{CH3} are the number of carbons in double bonds, methylene-, and methyl groups respectively; and V_{CH}, V_{CH2}, and V_{CH3} are the respective Koenig segmental volumes.[28] Considering that CaPLiLX size is in the range from 90 to 160 nm (as observed by TEM), that the thickness of CaP coating ranges from 20 to 40 nm [10] and the thickness of a bilayer is of ~4 nm, [29,30] a

simple geometrical calculation yields a bilayer volume of about 2.6×10^{7}- 7.0×10^{7} Å^3 for a liposome carrying the antibiotic LX. Therefore, each liposome is composed by *ca*. 2.0×10^{4} to 5.4×10^{4} DOPA molecules equivalent to 2.4×10^{-14}- 6.5×10^{-14} mg DOPA. Since 1 mg of DOPA molecules were contained in 1 mL suspension of liposomes (*see above*), a concentration in suspension of 1.5×10^{13} - 4.2×10^{13} liposome/mL is retrieved. Considering an encapsulated LX concentration of ~3.3 µg per ml of liposome suspension after coating, then an estimate of 7.9×10^{-14}- 2.2×10^{-13} µg LX/ liposome is obtained. Therefore, the minimal bactericidal concentration (MBC) of free LX needed to treat *S. aureus* strains (~1.0 µg/mL) (*see below*) is contained in ~ 8.8×10^{12} CaP-coated liposomes, that is *ca*. 40 % of the liposomes contained in 1 mL suspension.

The calcium concentration in the CaPLiLX suspension determined by ICP-OES was of 34.5 mg/kg (~34.5 µg/mL). Considering that all the liposomes are covered by the CaP shell and no calcium phosphate phase is formed separately (*vide supra*), about 8.2×10^{-13} -2.3×10^{-12} µg Ca/liposome can be estimated. Considering that the mineral phase is composed of amorphous dicalcium phosphate dyhydrate (DCP,$CaHPO_4.2H_2O$), of 2.31 gr/cm^3 density[31] a volume of 1.5×10^{6} -4.3×10^{7}Å^3 is calculated for the nanoshell from which a thickness of ~10 nm can be estimated, in good agreement with that observed in TEM images of empty CaPLi.[10]

3.3 Localization of the drugs within the liposome structure.

LX emission spectrum obtained from CaPLiLX aqueous suspensions upon 340 nm excitation (see Fig. 4a) is very broad, suggesting the localization of LX in different environments. In fact, a bilinear analysis suggests the contribution of three well differentiated emitters, denoted as E1, E2, and E3 with 16, 60 and 24 % contribution to the overall emission, respectively. The emission spectra of E1 (maximum emission at 430 nm) and E2 (maximum emission at 455 nm), see Fig. 4a, are in complete agreement with those obtained by TRES analysis for decay times of 1.7 ns and 6.5 ns, respectively. The E2 emission maxima and corresponding lifetime are in excellent agreement with those of LX

aqueous solutions of pH 7.4 showing an emission maximum (λ^{em}_{max}) at 460 nm with decay lifetime τ_{aq} of (6.2 ± 0.1) ns upon 341 nm excitation as also shown in Fig. 4a. E1 emission spectrum and decay lifetime are similar to those observed in a less polar media like hexane (τ_{hexane} = (1.4 ±0.1) ns and λ_{max} 425 nm, see Fig. 4a), in line with the fact that hexane might resemble the low polarity environment of the DOPA bilayer. The third component, E3, with an emission maximum at 495 nm may be attributed to the protonated levofloxacin molecule, LXH^+ [32] though an adsorbed specie on the CaP interface [33] and binding to divalent cations [34] cannot be discarded.

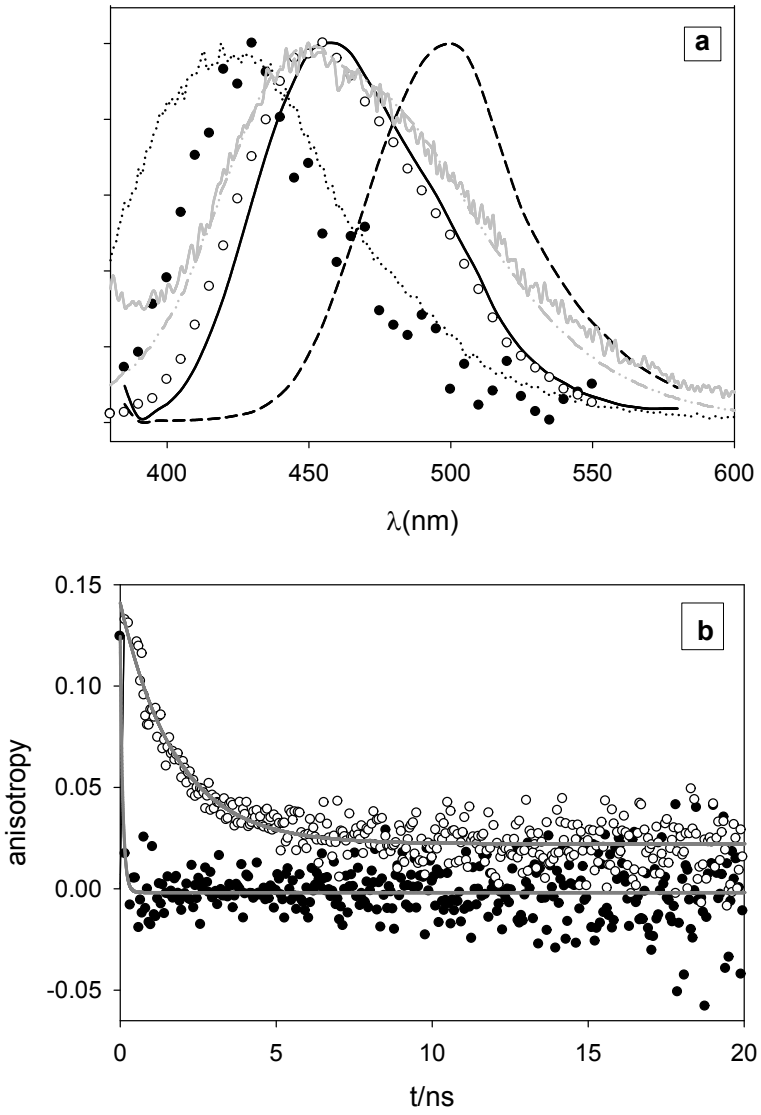

Fig. 4. (a) Emission spectra of: CaPLiLX aqueous solutions upon 341 nm excitation (grey solid lines) and fitting to three components (grey dashed lines); LX aqueous solutions of pH 7.4 (black solid line)

and pH 4(black dashed line); LX in hexane (black dotted line); emitting specie E1 (●) and emitting specie E2 (○). (b) Time-resolved fluorescence anisotropy decay LX (λ_{exc} = 341 nm) in aqueous media (●) and encapsulated in liposomes (○). The grey lines stand for the monoexponential fitting, see text.

Time resolved anisotropy experiments of LX and LiLX aqueous suspensions were performed upon 341 nm excitation. The time-resolved anisotropic decays could be well fitted to a monoexponential decay for both samples as shown in Fig. 4b. The rotational correlation times obtained for LX and LiLX samples are θ_{LX}=0.08 ± 0.09 ns and θ_{LiLX}=1.8 ± 0.5 ns, respectively. From these values and considering spherical species, [35] hydrodynamic radius (r_h) of 4.5 and 12.5 Å were estimated for LX and LiLX, respectively. While the value obtained for LX in aqueous solutions is of the order expected for small organic molecules, that obtained for LX encapsulated in the liposome suggests a motional restriction as also reported for norfloxacin in AOT reverse micelles.[36]

Altogether, the previous results support LX localization within the liposome, with a preferential location in the liposome aqueous core and minor amounts located within the lipid bilayer of the liposomes and adsorbed to the CaP shell. A similar distribution was reported for ciprofloxacin in L-α-1, 2-Dipalmitoyl-sn-glycerophosphocholine liposomes.[37]

3.4 Drug release profiles in aqueous media as a function of pH and ions- containing media.

Release profiles of free LX in aqueous solution from membrane bags immersed in PBS occurs almost completely in less than 3 hours under conditions of constant stirring and ionic strength of 0.16 M and pH 7.4, as shown in Fig. 5 *inset*. However, in acetate buffer solution of I=0.009 M and pH 4.35, the drug was completely transferred to the media in less than one hour (see SI, Fig. S3). Thus, these observations suggest that diffusion outside the dialysis membrane may limit LX release studies from CaPLiLX for liberation times of a few hours, depending on the release media.

Encapsulated drug in CaPLiLX vesicles in PBS, acetate buffers and SBF media (see Fig. 5) showed a fast-initial drug release of *ca.* 35-45% in all the studied media during the first hours. This burst release is coincident with that observed for a sample of LX adsorbed in the outer layer of empty liposomes in PBS media.[33,38,39] Since the burst release takes place in the same time window than diffusion of LX from the dialysis membrane as may be observed in Fig. 5(*inset*) for experiments in PBS, care should be taken in the analysis of the drug release mechanisms from these experiments.

To obtain some information on the mechanisms involved, the fraction of drug released at time t (RR) up to RR= 0.6 of all curves in Fig. 5 were fitted to Korsmeyer-Peppas (KP) model developed on the basis of water-soluble drug release from polymeric matrices and also applied to porous CaP-ceramic materials and composites.[40,41] To that purpose, curves of RR *versus* time were fitted (see lines in Fig. 5) to the relation $RR = k_{KP} \times t^n$, where k_{KP} is the release rate constant which depends on the structural and physical characteristics of the carrier and the drug, and n is the release exponent which depends on the drug release mechanism and on the carrier geometry. The fitted parameters are displayed in SI Table S1. Obtained k_{KP} values are, within the experimental error, similar for surface adsorbed LX in CaPLi and CaPLiLX, both, in PBS (pH 7.4) and acetate (pH 4.35) buffers, thus supporting the same nature of the vehicle in all cases. On the other hand, values of the diffusional exponent n were, within the experimental error, of *ca.* 0.11 for all experiments. Considering that values of $n = 0.43$ are reported as the limiting value for a Fickian diffusion mechanism from monodispersed spherical samples,[42] the lower values of n observed here may be partly related to the size distribution polydispersity of the particles which leads to an accelerated release process at short times and a decelerated transport at long times.[42] Interestingly, dialysis of free LX show $k_{KP} = 0.59$ different from that of CaPLi and CaPLiLX, and $n=0.6 \pm 0.1$ which is related to a typical diffusional mechanism.

Altogether, these results further support that, any LX release form CaPLiLX vesicles in PBS and acetate buffers occurs from adsorbed LX on the CaP outer shell of the nanostructure. Such drug release occurs within the same time window of solvent free LX diffusion out of the dialysis membrane.

View Article Online
DOI: 10.1039/C9NJ00414A

Considering that, after the first burst no further LX release is observed from CaPLiLX in PBS and acetate buffers and since liberation of surface adsorbed LX from CaPLi is complete in this time window, it may be concluded that surface adsorbed LX on the vehicle outer shell accounts for a 40 to 45 % of total LX contained in CaPLiLX.

A different situation is observed for CaPLiLX in SBF where a preferential drug release of *ca.* 90% drug after 50 hs is observed, thus indicating that SBF ionic composition is responsible for the improved release. Also, $k_{KP} = 0.55$ obtained in SBF (pH 7.4) similar to that of solvent free LX, seems to support an alteration in the nanocarrier facilitating the delivery of the drug.

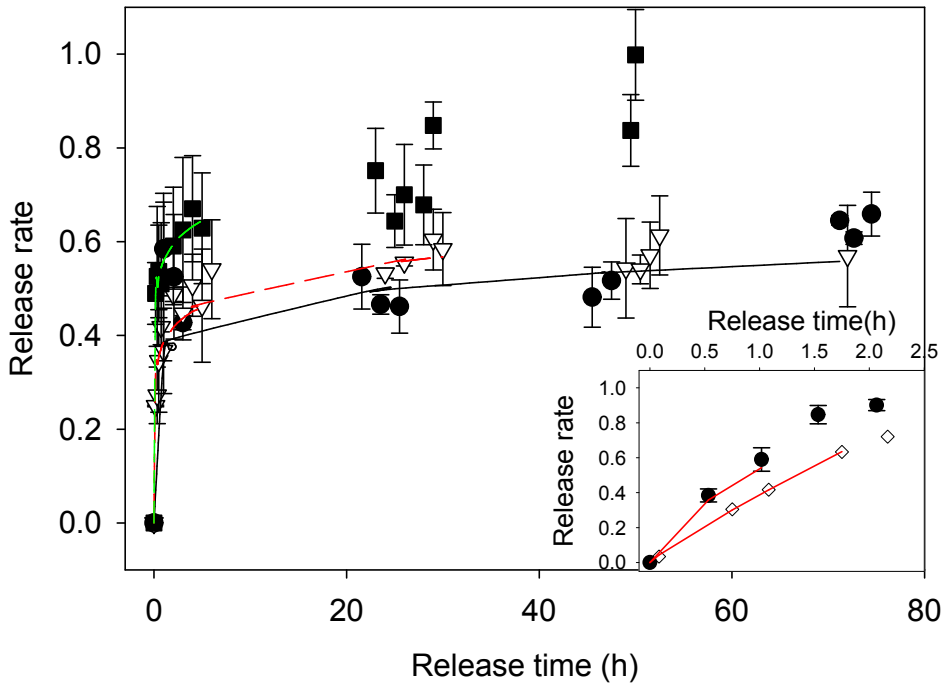

Fig. 5. Release profiles for LX entrapped in CaPLiLX in PBS (black circles), acetate buffer solution (white triangles) and SBF (black squares). Curves stand for the fitting to Kosmeyer-Peppas model (up to *ca* 0.6). *Inset*: Release of LX adsorbed in empty CaPLi in PBS (black diamonds) and solvent free LX diffusion out of the dialysis membrane in PBS (white diamonds). Red curves stand for the fitting to Kosmeyer-Peppas model (up to *ca* 0.6). Error bars stands for SD.

View Article Online
DOI: 10.1039/C9NJ06414A

3.5 Proving the release mechanism in SBF.

Considering the amorphous character of the CaP coating as determined by XRD experiments, we hypothesized that the presence of Ca^{2+} and Mg^{2+} ions in SBF may be involved in the improved drug release from the nanocarriers. In a first instance, the transformation of the amorphous calcium phosphate (ACP) to crystalline apatite in the presence of Ca^{2+} and Mg^{2+}, in line with the reported transformation of amino acid containing amorphous calcium phosphates into apatite when immersed in calcium containing solution,[43] was explored by XRD and WAXS.

The XRD pattern (Fig. S2) obtained for CaPLiLX deposited on a glass slide from a solution containing Ca^{2+} (as $CaCl_2$ 0.05 M) is coincident with that obtained in the absence of the divalent ion salt. Both samples present a broad band at 2θ~25ºC typical of an amorphous sample. Also, WAXS experimental patterns shown in Fig. 3b, present the same broad band in the range 20-40 º typical of amorphous samples, for both CaPLiLX, and CaPLiLX suspended in a Ca^{2+} solution (as $CaCl_2$ 0.05 M). Altogether, XRD and WAXS data confirm that no significant formation of a calcium phosphate crystalline phase occurs when the CaP shell gets in contact with calcium ions.

Formation of a coordination complex between surface carboxyl groups of nanoparticles and Ca^{2+} ions is well-reported in the literature.[44] Considering that our CaP nanoshells are surface-terminated by the attachment of CEPA moieties, carboxyl groups are abundant on the nanoshell surface (*see* ATR-FTIR results). The bonding of Ca^{2+} ions to these carboxyl surface groups may trigger the disassembling of the whole structure leading finally to an improved drug release. In that sense, it was demonstrated that the presence of divalent cations as Ca^{2+} and Mg^{2+} can lead to the collapse of carboxylic terminated brushes of spherical colloids also provoking their aggregation.[45,46] With the purpose of confirming such hypothesis, the hydrodynamic diameter and surface charge of CaPLiLX sample were evaluated in the presence of 0.05M of divalent cations (Ca^{2+} and Mg^{2+}), as depicted in SI, Table S2. An increase of the hydrodynamic diameter of the nanoshells and the consequent decrease in the electrophoretic mobility was observed in the presence of both, Ca^{2+} and Mg^{2+}, supporting the formation of

View Article Online
DOI: 10.1039/C9NJ00414A

agglomerates mediated by divalent cations-carboxyl complexes.[47] Moreover, a significant increase of PDI (≥ 0.75) was also observed in the presence of divalent cations, which may be caused by increased nanocarrier fusion and aggregation. Considering these results and the enhanced LX release in SBF (*see above*), the effect of divalent cations on the agglomeration and consequent disassembling of the nanoshells in solution is strongly supported. In view of these results and bearing in mind the aim to develop a drug nanocarrier responsive to Ca^{2+}-surfaces, we further explored the behavior of the CaP nanoshells over Ca^{2+}- enriched surfaces by diverse microscopy studies.

3.6 Interaction of nanoshell with Ca^{2+} rich surfaces.

AFM topographic images of CaPLiLX nanoshells deposited on mica surfaces revealed spherical-like particles and some agglomerates (Fig. 6a). The height profile showed well defined spheres with an average height of 9.8 nm and an average diameter of 132.5 nm, in line with DLS, and electron microscopies results. On the other hand, images of CaPLiLX dropped on mica with the previous deposition of Ca^{2+} (Fig. 6b and 6c) showed the aggregation, crushing and dragging of the nanoshells on the surface. In addition, the irregular shapes registered by the probe are evident in the height profile, for both 5.0 (Fig. 6b) and 1.2 μm (Fig. 6c), where a height of *ca.* 4 nm is displayed, in coincidence with that observed for a phospholipid bilayer thickness.[29,30] The result suggests the rupture of the CaP shell when the sample is in contact with a Ca^{2+} rich surface, leaving the liposomes exposed and leading to their disruption on the surface.

View Article Online
DOI: 10.1039/C9NJ06414A

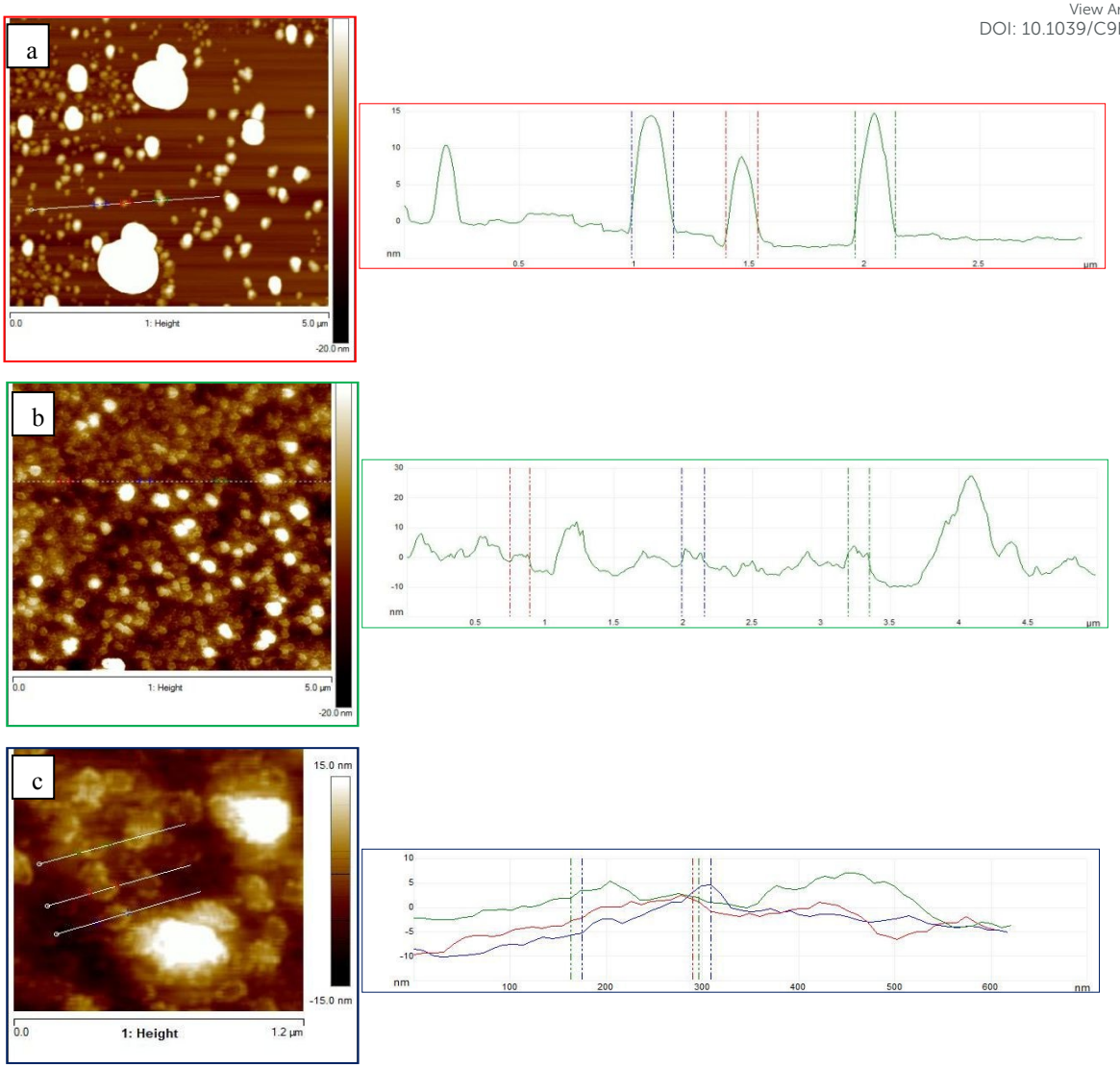

Fig. 6. AFM images of CaPLiLX on mica (a) and on Ca^{2+} mica modified surface (b and c).

In order to explore the calcium speciation and contact time on the CaP nanoshells interaction with calcium-enriched surfaces, SEM images of CaPLiLX dropped on BGS and Ap-BGS were obtained after 10 and 120 minutes of contact (Fig. 7). Unmodified BGS scaffold's image is also displayed (Fig. 7, *inset*). Although nanoshells were observed on both Ap-modified and BGS unaltered surfaces, a noticeable accumulation of CaPLiLX over Ap-BGS was observed for both contact times. On the other hand, nanoshells observed in the unmodified BGS, showed uniform distribution over the surface. The images taken at different contact times showed the immediate accumulation (10 min) of the nanoshells

on the Ap-BGS surface. The results suggest that the nanoshells have an important interaction with apatite-enriched scaffolds and a preferable accumulation is taking place over calcium- modified surface.

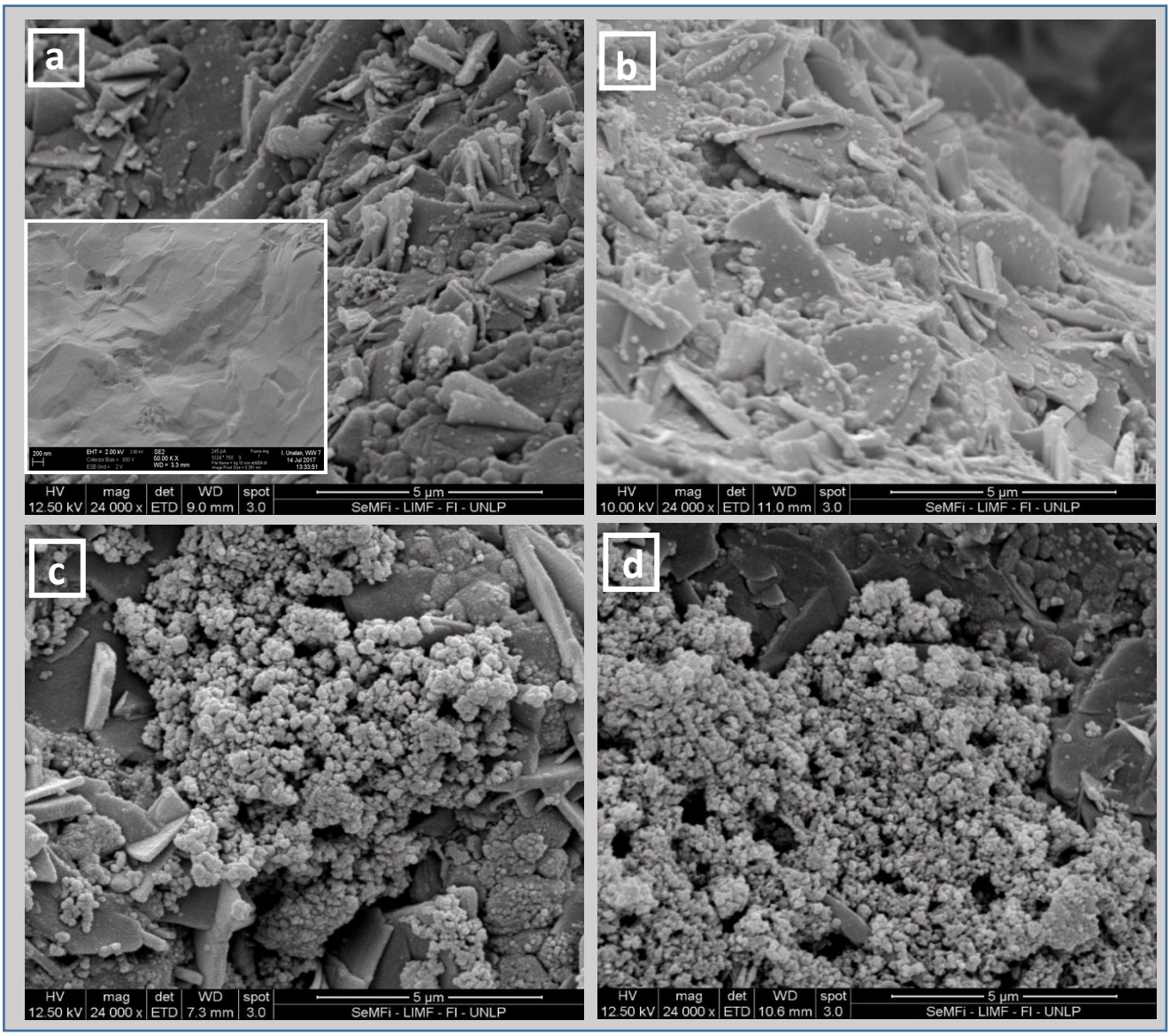

Fig. 7. SEM images of (a) CaPLiLX over BGS after 10 min and (b) after 120 min. (c) CaPLiLX over Ap-BGS after 10 min and (d) after 120 min of contact time. *Inset*: Image of unmodified BGS scaffold.

Finally, to confirm the release of the content when the CaP nanoshells are disrupted, a new suspension of CaP coated liposomes containing acridine orange fluorophore (CaPLiAO) was prepared and

observed in an epifluorescence microscope. The release of acridine orange was studied on uncoated and Ap-coated glass slides observing the morphology and changes in fluorophore emission intensity at different contact times. To that purpose, 2 mL of CaPLiAO suspension was deposited over the glasses and the whole system observed immediately (0 min) and after 10 minutes and 180 min of contact time. Control images were also obtained before adding the CaPLiAO suspension to check the absence of emission in unmodified and Ap-modified glass surfaces. The images, taken in triplicate, showed the release of the AO fluorophore from the CaP nanoshells on the Ap-modified glasses since the first minutes of contact leading to the staining of the entire Ap-modified glass surface after 180 min (Fig. 8). On the other hand, the emission observed over the unmodified surface is centered in small areas corresponding to the fluorophore contained in nanoshells or their aggregates.

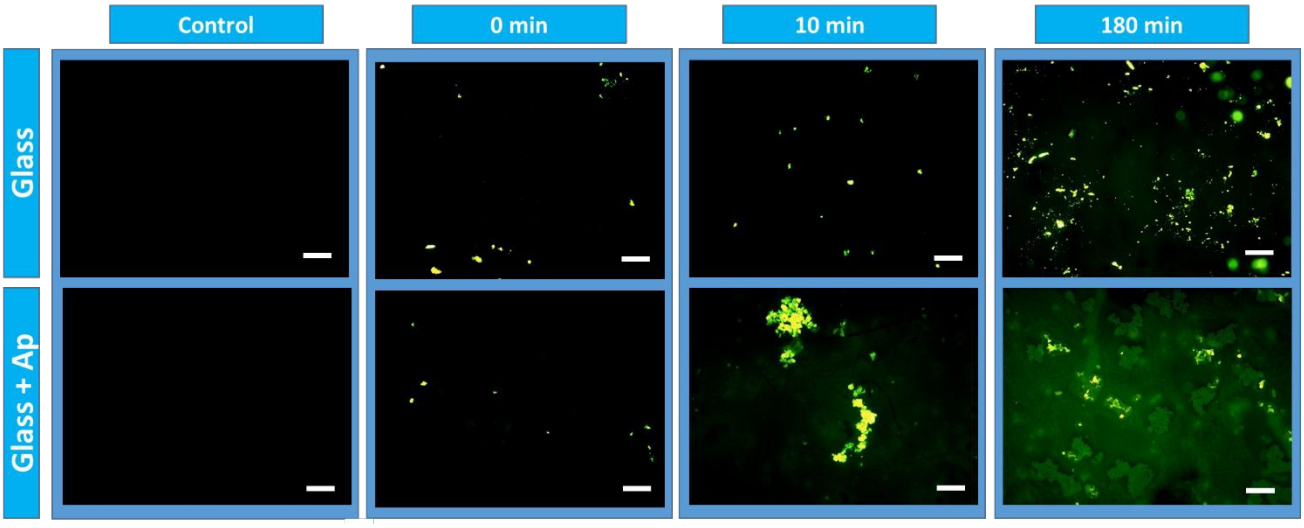

Fig. 8. Epifluorescence images of CaPLiAO interaction with Ap-modified (below) and unmodified (above) glass at 0 min, 10 min and 180 min of contact time. Control images are also displayed. Scale bar is 10 µm.

The fluorescence intensity as a function of surface and time was evaluated by calculation of the image covered area using Image J software. The results presented in Fig. S4 clearly demonstrated the

View Article Online
DOI: 10.1039/C9NJ06414A

enhanced release of the AO fluorophore from the CaP nanoshell deposited over Ap-modified surface as observed by the naked eye.

Altogether, atomic force, scanning electron and epifluorescence microscopy results support the hypothesis that the CaP shells accumulate immediately after contact and break over calcium containing surfaces, exposing the liposomes, which are dissembled, releasing their drug content to the surroundings in few hours.

3.7 Time-kill curve of planktonic *S. aureus*.

In order to confirm that the nanoshells are capable of transporting and maintaining the antibiotic activity of encapsulated LX, time-kill curve experiments were performed with LX and CaPLiLX. *In vitro* susceptibility of *S. aureus* to LX was determined on planktonic cells. MIC and MBC (see Experimental Section) values obtained for *S. aureus* were 0.5 μg/mL and 1.0 μg/mL, respectively. Based in these results, LX concentration for time-kill assay was evaluated at MBC (2x MIC) value.

Time-kill curve for *S. aureus* showed that bactericidal activity was reached at 6 hours and total eradication of bacteria was achieved within 24 h for both free LX and CaPLiLX (Fig. 9). However, a difference was observed in the kinetics of the antimicrobial activity between the CaPLiLX sample and free LX. Although the antimicrobial activity is preserved for the encapsulated formulation, a small difference was observed in the first 3 hours. These results are consistent with the sustained release of LX observed from the nanoshells in solution, reaching about 40 % release in 3h in solution (~1.3 μg LX/mL) (*see* Fig. 5) which explains that both, CaPLiLX and LX solution, exhibited similar antimicrobial action against *S. aureus*.

View Article Online
DOI: 10.1039/C9NJ06414A

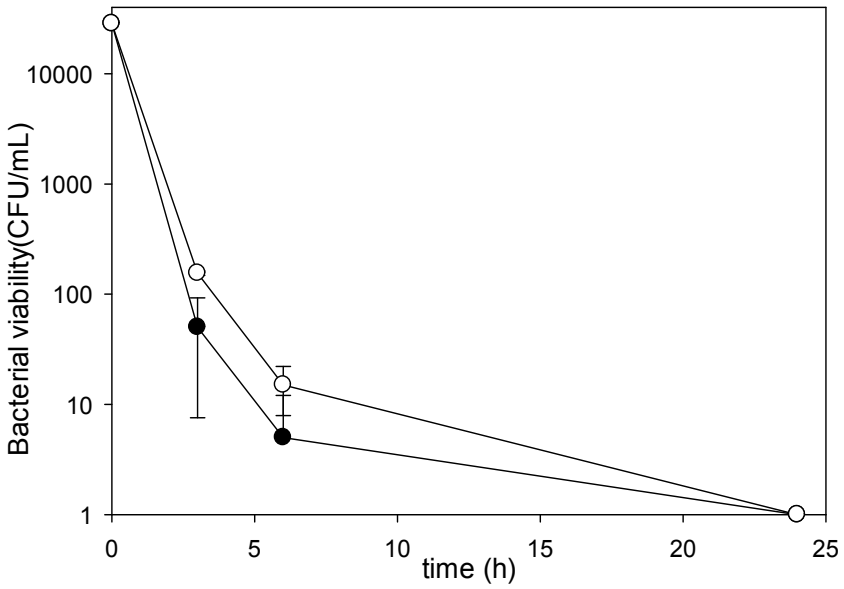

Fig. 9. Effects of free LX and CaPLiLX on the viability of *S. aureus* ATCC 25923. The *in vitro* time-kill experiments were performed in duplicate; mean and SD values were plotted. 2x MIC LX (●) and CaPLiLX formulation(○). CFU: colony forming unit.

Although the surface charge of the CaPLiLX nanoshell is negative, the nanoshells interact with the *gram-positive* bacterial outer membranes, leading to bacterial killing. This interaction was previously observed for acridine orange and 5,10,15,20-Tetrakis(1-methyl-4-pyridinio)porphyrin containing CaPLi nanoshells.[10] The teichoic acid and the peptidoglycan components of the bacterial cell wall contribute to the negative charge of the staphylococcal cell surface. Moreover, these phosphate-containing and sugar polymers are the major bacterial components for sequestering metal ions from the environment, mostly Ca^{2+} and Mg^{2+}.[48] In our previous work, we hinted that the phosphate groups of the bacterial cell wall and the external calcium and magnesium ions may be responsible for the preferential accumulation of the nanoshells in *S. aureus* biofilms and smears. As was broadly demonstrated in this work, calcium and magnesium ions also play an important role in the agglomeration and consequent disassembling of the nanoshells. We may conclude that the localization of these divalent metal ions on the vicinity of the bacterial wall may attract the nanoshells and finally

provoke their disruption and antibiotic content release near the bacterial cell, consistent with our proposed release mechanism.

4. CONCLUSIONS

Highly stable CaP-coated liposomes of 90 -160 nm size were synthesized and their capability of incorporating model drugs as the antibiotic Levofloxacin demonstrated. The drug distribution inside the aqueous core and into the bilayers was determined by steady state, time resolved and anisotropy fluorescence measurements. Drug adsorption on the CaP surface was also confirmed by release profiles.

The amorphous character of the CaP shell of the vehicles is a decisive condition triggering the release of any included and surface adsorbed drug. It is well known from the literature, that amorphous CaP is more easily dissolved than crystalline calcium phosphate solids.[13,49,50] The higher water content of CaP amorphous phase compared to crystalline phases may favor the entrance of the water molecules from the solvent, enhancing its dissolution. Moreover, drug release from the surface of CaP solid nanoparticles depends on the particle phase, the surface impurities, the interaction with water and the nature of the drug. The fast release observed here for adsorbed LX on the surface of CaPLiLX and CaPLi, may be due to a weak adsorption of LX on the amorphous CaP external shell. Whether such burst release is not a desired condition, the dialysis may be a good option for nanoshells purification. Because surface adsorption is involved in the drug inclusion in CaPLi vehicles, other farmaceuticals might show a different behavior, as is the case of the AO dye.[10]

The release response of CaP shells to Ca^{2+} and Mg^{2+} cations in solution showed that these divalent ions were able to complex the nanoshell surface provoking aggregation and being able to trigger the disruption of the CaP shell. In line with this behavior, an immediate response of CaP nanoshells localization to Ca^{2+} and hydroxyapatite-modified surfaces was observed, followed by the CaP shell disassembling and fusion of the liposome leading to the release of their content in few hours.

Finally, the potential of novel CaP-based nanocarriers for drug delivery applications was demonstrated in bacterial time-kill experiments of *S. aureus* planktonic cells as similar bacterial time-kill curves for CaPLiLX formulations and the free antibiotic were obtained probably as the consequence of the interaction of divalent cations present in the vicinity of the *gram-positive* bacteria with CaPLiLX.

Altogether, our work clearly reveals the potential of amorphous calcium organophosphate nanoshells for specific transport, localization and drug delivery to calcium-enriched surfaces, as bone tissues.

ACKNOWLEDGMENTS

This work was financially supported by ANPCyT (PICT2014-2746) and Universidad Nacional de La Plata. D.J.P.E. and M.L. Dittler thanks CONICET, Argentina, for their graduate studentship. M.L.Dell'Arciprete, M.C.G., A. M. and E.P. are research members of CONICET, Argentina.

Aldo R. Boccaccini from the Institute of Biomaterials, University of Erlangen-Nuremberg, Germany, is thanked for the knowhow in the preparation of the glass-based scaffolds and for his useful discussions.

Alberto Caneiro from Y-TEC and Gabriel Lavorato from INIFTA are thanked for their valuable help in preparation and obtention of HR-STEM images and EDS analysis.

ELECTRONIC SUPPLEMENTARY INFORMATION (ESI)

Characterization Methods; Electron microscopies images of nanoshells; X-Ray Diffraction patterns of CaP nanoshells; Release profiles for free LX in acetate buffer; Parameters of the fitting of the release profiles to Korsmeyer-Peppas and Weibull model; Diameter and electrophoretic mobility for the nanoshells in the absence and in the presence of Ca^{2+} and Mg^{2+};Fluorescence covered area on glass slides with added nanoshells as a function of contact time.

REFERENCES

1 Y. H. Choi and H.-K. Han, *J. Pharm. Investig.*, 2018, **48**, 43–60.

2 J. V Natarajan, C. Nugraha, X. W. Ng and S. Venkatraman, *J. Control. Release*, 2014, **193**, 122–138.

3 M. Liu, H. Du, W. Zhang and G. Zhai, *Mater. Sci. Eng. C*, 2017, **71**, 1267–1280.

4 X. Wang and W. Li, *Nanotechnology*, 2016, **27**, 1–8.

5 Y. Zhang, T. Sun and C. Jiang, *Acta Pharm. Sin. B*, 2018, **8**, 34–50.

6 C. J. Kowalczewski and J. M. Saul, *Front. Pharmacol.*, 2018, **9**, 1–15.

7 Q. Xu, Y. Tanaka and J. T. Czernuszka, *Biomaterials*, 2007, **28**, 2687–2694.

8 D. Huang, B. He and P. Mi, *Biomater. Sci.*, 2019.

9 H. Y. Erbil, *Surface Chemistry of Solid and Liquid Interfaces*, Blackwell Publishing Ltd, Oxford, First Edit., 2006.

10 I. Rivero Berti, M. L. Dell' Arciprete, M. L. Dittler, A. Miñan, M. Fernández Lorenzo de Mele and M. Gonzalez, *Colloids Surfaces B Biointerfaces*, 2016, **142**, 214–222.

11 H. T. Schmidt, B. L. Gray, P. A. Wingert and A. E. Ostafin, *Chem. Mater.*, 2004, **16**, 4942–4947.

12 C.-H. Yeo, S. H. S. Zein, A. L. Ahmad and D. S. McPhail, *Ceram. Int.*, 2012, **38**, 561–570.

13 V. Uskoković and T. A. Desai, *J. Biomed. Mater. Res. - Part A*, 2013, **101 A**, 1416–1426.

14 Q. Z. Chen, I. D. Thompson and A. R. Boccaccini, *Biomaterials*, 2006, **27**, 2414–2425.

15 M. L. Dittler, I. Unalan, A. Grünewald, A. M. Beltrán, C. A. Grillo, R. Destch, M. C. Gonzalez and A. R. Boccaccini, *Colloids Surfaces B Biointerfaces*, 2019, **182**, 110346.

16 H. G. Enoch and P. Strittmatter, *Proc Natl Acad Sci USA*, 1979, **76**, 145–149.

17 C. J. M. Stewart, *Anal. Biochem.*, 1980, **104**, 10–14.

18 X. Zhang, P. Sun, R. Bi, J. Wang, N. Zhang and G. Huang, *J. Drug Target.*, 2009, **17**, 399–407.

19 P. Wayne, *Performance Standarts for Antimicrobial Disk Susceptibility Tests; Approved Standard; 9 Edition*, 2006, vol. 26.

20 P. J. Petersen, P. Labthavikul, C. H. Jones and P. A. Bradford, *J. Antimicrob. Chemother.*, 2006, **57**, 573–576.

21 X.-S. Tao, Y.-G. Sun, X.-J. Lin, L.-L. Hu, T.-Q. Sun, D. Zhang, A.-M. Cao and L.-J. Wan, *Dalt. Trans.*, 2018, **47**, 12843–12846.

22 E. G. Palacios, A. J. Monhemius and G. Jua, *Hydrometallurgy*, 2004, **72**, 139–148.

23 M. Manoj, D. Mangalaraj, N. Ponpandian and C. Viswanathan, *RSC Adv.*, 2015, **5**, 48705–48711.

24 D. Muthu, M. Gowri, G. Suresh Kumar, V. S. Kattimani and E. K. Girija, *New J. Chem.*, 2019, **43**, 5315–5324.

View Article Online
DOI: 10.1039/C9NJ06414A

25 V. Cadež, D. M. Lyons, D. Kralj and M. D. Sikiri, *Crystals*, 2018, **8**.

26 S. V Dorozhkin, *Acta Biomater.*, 2010, **6**, 4457–4475.

27 G. A. Islan, P. C. Tornello, G. A. Abraham, N. Duran and G. R. Castro, *Colloids Surfaces B Biointerfaces*, 2016, **143**, 168–176.

28 B. W. Koenig and K. Gawrisch, *Biochim. Biophys. Acta*, 2005, **1715**, 65–70.

29 Z. V. Feng, T. A. Spurlin and A. A. Gewirth, *Biophys. J.*, 2005, **88**, 2154–2164.

30 N. Delorme and A. Fery, *Phys. Rev. E - Stat. Nonlinear, Soft Matter Phys.*, 2006, **74**, 3–5.

31 C. Holt, P. A. Timmins, N. Errington and J. Leaver, *Eur. J. Biochem.*, 1998, **252**, 73–78.

32 A. Polishchuk, T. Emelina, E. Karaseva, O. Cramariuc, V. Chukharev and V. Karasev, *Photochem. Photobiol.*, 2014, **90**, 79–84.

33 C. F. Marques, A. C. Matos, I. A. C. Ribeiro, L. M. Gonçalves, A. Bettencourt and J. M. F. Ferreira, *J Mater Sci Mater Med*, 2016, **27**, 1–12.

34 V. Uivarosi, *Molecules*, 2013, **18**, 11153–11197.

35 J. R. Lakowicz, *Principles of Fluorescence Spectroscopy*, Springer, New York, Third Edit., 2006.

36 B. K. Paul, N. Ghosh, A. Tewary and S. Mukherjee, *Proc. Indian Natl. Sci. Acad.*, 2016, **82**, 1259–1269.

37 J. Hernández-Borrell and M. T. Montero, *Int. J. Pharm.*, 2003, **252**, 149–157.

38 G. D. Venkatasubbu, S. Ramasamy, V. Ramakrishnan and J. Kumar, *Biotech*, 2011, **1**, 173–186.

39 A. Jain and S. K. Jain, *Chem. Phys. Lipids*, 2016, **201**, 28–40.

40 S. Dash, P. N. Murthy, L. Nath and P. Chowdhury, *Acta Pol. Pharm. Drug Res.*, 2010, **67**, 217–223.

41 U. Gbureck, E. Vorndran and J. E. Barralet, *Acta Biomater.*, 2008, **4**, 1480–1486.

42 P. L. Ritger and N. A. Peppas, *J. Control. Release*, 1987, **5**, 23–36.

43 N. Ikawa, T. Kimura and T. Sano, *J. Mater. Chem.*, 2009, **19**, 4906–4913.

44 A. Ethirajan, U. Ziener and K. Landfester, *Chem. Mater.*, 2009, **21**, 2218–2225.

45 A. Ezhova and K. Huber, *Macromolecules*, 2016, **49**, 7460–7468.

46 R. J. Nap, E. Gonzalez Solveyra and I. Szleifer, *Biomater. Sci.*, 2018, **6**, 1048–1058.

47 D. Li, Z. Fang, H. Duan and L. Liang, *Biomater. Sci.*, 2019, **7**, 2841–2849.

48 K. J. Thomas and C. V. Rice, *Biochim. Biophys. Acta - Biomembr.*, 2015, **1848**, 1981–1987.

49 V. Uskoković, *J. Mater. Chem. B*, 2019, **7**, 3982–3992.

50 V. M. Wu and V. Uskoković, *Biochim. Biophys. Acta - Gen. Subj.*, 2016, **1860**, 2157–2168.

View Article Online
DOI: 10.1039/C9NJ06414A

Table of Content

We show that amorphous calcium organophosphate nanoshells are prone to agglomerate and disassemble when Ca^{2+} ions are present in the solution and on surfaces, wich have great implications for targeting and controlled drug release in Ca-rich environments, such as bone tissues.